Absence of spontaneous time-reversal symmetry breaking and ferromagnetism in superconducting $NiBi_3$ single crystal

Jingyuan Wang,[1] Camron Farhang,[1] Di Yue,[2] Xiaofeng Jin,[2] Xiangde Zhu,[3] and Jing Xia[1,*]

[1]*Department of Physics and Astronomy, University of California, Irvine, California 92697, USA*

[2]*Department of Physics, Fudan University, Shanghai 200433, China*

[3]*Anhui Province Key Laboratory of Condensed Matter Physics at Extreme Conditions, High Magnetic Field Laboratory of the Chinese Academy of Sciences, Hefei, 230031 Anhui, China*

(Received 22 August 2022; accepted 19 December 2022; published 13 January 2023)

Recent experiments have pointed to chiral *p*-wave-like superconductivity in epitaxial Bi/Ni bilayers that are spontaneously time-reversal symmetry breaking (TRSB), making it a promising platform for exploring physics useful for topologically protected quantum computing. Quite intriguingly, evidence has emerged that, in nonepitaxial Bi/Ni bilayers, superconductivity arises due to the formation of $NiBi_3$, which has been reported to host coexisting ferromagnetic and superconducting orders at the surface. We perform high-resolution surface magneto-optic Kerr effect measurements using a Sagnac interferometer on single-crystal $NiBi_3$ and find no sign of any spontaneous Kerr signal except for contributions from trapped vortices. This strongly indicates the absence of TRSB in $NiBi_3$, whether due to TRSB in the superconducting state or any coexisting ferromagnetism, and we conclude that the superconductivity found in nonepitaxial Bi/Ni is distinctively different from that in epitaxial Bi/Ni.

DOI: 10.1103/PhysRevB.107.024415

I. INTRODUCTION

The quest to build a reliable quantum computer has stimulated intense research into quantum phases with quasiparticles that obey non-Abelian exchange rules and can be used for topologically protected quantum computing [1]. Such quasiparticles would exist as Majorana bound states in the vortex cores of a chiral *p*-wave superconductor [1,2], which is an electronic analog to the A-phase of superfluid He^3 [3] and breaks time-reversal symmetry (TRS). In the prototypical chiral *p*-wave superconductor Sr_2RuO_4 ($T_C \approx 1.5$ K), although TRS-breaking (TRSB) has been confirmed by muon spin relaxation (μSR) [4], surface magneto-optic Kerr effect (SMOKE) measurements using a Sagnac interferometer [5], and μSR under strain [6], the *p*-wave aspect has been challenged by the recent nuclear magnetic resonance evidence [7] for an even-parity superconducting order parameter. In addition, a magnetic competing order has been identified in close proximity [8] by μSR [6] and elastocaloric effects [8], making the picture of Sr_2RuO_4 rather complicated.

Superconducting epitaxial Bi/Ni bilayers provide a promising alternative candidate for chiral *p*-wave superconductivity. It was initially found in tunneling measurements that Bi layers deposited on Ni layers become superconducting with $T_C \approx 4$ K [9], and there are coexisting superconducting and ferromagnetic gaps when tunneling from the Ni side [10]. More recently, in high-quality Bi/Ni bilayers grown by molecular beam epitaxy (MBE), superconducting quantum interference device (SQUID) measurements [11] show evidence for chiral superconductivity and the formation of chiral domains. SMOKE measurements using a Sagnac interferometer [12] conducted on the Bi side reveal spontaneous TRSB in the superconducting state, where chirality can be trained by a small magnetic field ∼100 Oe. Assuming that superconductivity exists only in the top Bi surface away from Ni, we have proposed a $d_{xy} \pm id_{x^2-y^2}$ superconducting order parameter, which is the lowest angular momentum state allowed by this surface symmetry [12]. This hypothetical restriction was soon corrected by a time-domain terahertz spectroscopy experiment [13] that identified a nodeless superconductivity extending over the entire Bi/Ni bilayer. Their data also rule out the odd-frequency pairing [14], which is natural for a superconductor-ferromagnet interface. These experimental findings collectively point to chiral *p*-wave superconductivity in strongly spin-orbit-coupled epitaxial Bi/Ni bilayers [15], whose properties can in principle be engineered by the growth parameters (thickness, strain, and doping) to optimize the conditions for hosting Majorana particles.

Real materials are complex. A radically different picture has emerged in Bi/Ni bilayers fabricated using other methods, highlighting the role of the intermetallic compound $NiBi_3$. $NiBi_3$ impurities were first detected in thermally evaporated Bi/Ni bilayers by x-ray diffraction [16] and were proposed as the source for the observed superconductivity. Later studies on pulse-laser-deposited (PLD) [17] and sputter-deposited [18] Bi/Ni bilayers show the absence of superconductivity in as-grown samples without $NiBi_3$ impurities. By changing the deposition temperature [17] or by weeks of annealing [18], these samples develop superconductivity coincident with the formation of $NiBi_3$. As a known type-II *s*-wave superconductor with $T_C \approx 4$ K [19,20], $NiBi_3$ should be TRS invariant,

*xia.jing@uci.edu

but there are reports of coexisting ferromagnetism and superconductivity in $NiBi_3$. Extrinsic ferromagnetism was found in flux-grown $NiBi_3$ crystals due to amorphous Ni impurities [21]. Intrinsic magnetic orders were proposed at the surface due to modifications of surface electronic band structures [22]: SQUID magnetometry has identified ferromagnetism in $NiBi_3$ nanostrains (200 nm) with high surface fraction [22]; electron spin resonance has detected no ferromagnetism but found surface-induced magnetic fluctuations in single-crystal $NiBi_3$ [23].

Although these reports of magnetic orders in $NiBi_3$ differ quantitatively from the TRSB observed in epitaxial Bi/Ni bilayer by Sagnac interferometry [12], and the coexistence of ferromagnetism and superconductivity often leads to odd-frequency pairing [14] that is inconsistent with terahertz time-domain spectroscopy data [13], it is sometimes argued that the observed unconventional superconductivity in epitaxial Bi/Ni bilayers may come from superconducting $NiBi_3$ impurities that have surface-induced ferromagnetism. Does $NiBi_3$ break TRS? Is it ferromagnetic near the surface? Above all, do epitaxial and nonepitaxial Bi/Ni bilayers host identical or distinct superconducting states? These fundamental questions can be addressed by performing a definitive determination of the TRS and magnetic properties of single-crystal $NiBi_3$, especially near the surface.

II. EXPERIMENT

SMOKE [24,25] measurements performed by a zero-area loop fiber optic Sagnac interferometer [26] are ideally suited for performing such a definitive test of TRSB and ferromagnetism near the surface of $NiBi_3$. Probing the sample surface with an optical penetration depth δ that is typically a few nanometers for conductors [24,25], SMOKE has proven to be a powerful probe for surface magnetization. Primarily for detecting even smaller Kerr signals that arise in unconventional superconductors, we have introduced a zero-area loop [26] fiber optic Sagnac interferometer [27] that measures directly the nonreciprocal phase difference $\theta_{nr} = 2\theta_K$ between counterpropagating circularly polarized light beams, where θ_K is the Kerr rotation. This approach fundamentally rejects polarization rotations due to non-TRSB effects such as linear and circular dichroism [28]. This design has pushed the Kerr resolution from the microradian (μrad) [24,25] to the tens of nanoradians (nrad) level [5], allowing us to identify TRSB in various unconventional superconductors such as Sr_2RuO_4 [5] and Bi/Ni bilayers [12]. Scanning imaging capability with micrometer spatial resolution has allowed us to discover ferromagnetism in two-dimensional (2D) van der Waals layers [29] and to control magnetism in 2D structures [30]. We use a scanning Sagnac microscope operating at 1550 nm wavelength as illustrated in Fig. 1(a). The interferometer itself is located at room temperature. The piezoscanner [31] is mounted inside a cryostat with 1.8 K base temperature and 9 T magnetic field capability. A polarization maintaining fiber delivers lights of orthogonal linear polarizations into the high vacuum sample space inside the cryostat. A cryogenic quarter wave ($\lambda/4$) plate converts these light beams into circular polarizations of opposite chiralities that will interact with the sample surface and detect TRSB. Figure 1(b) shows a 16-h measurement on a silver mirror demonstrating 10 nrad Kerr resolution that is limited by long-term drifts in optics and electronics.

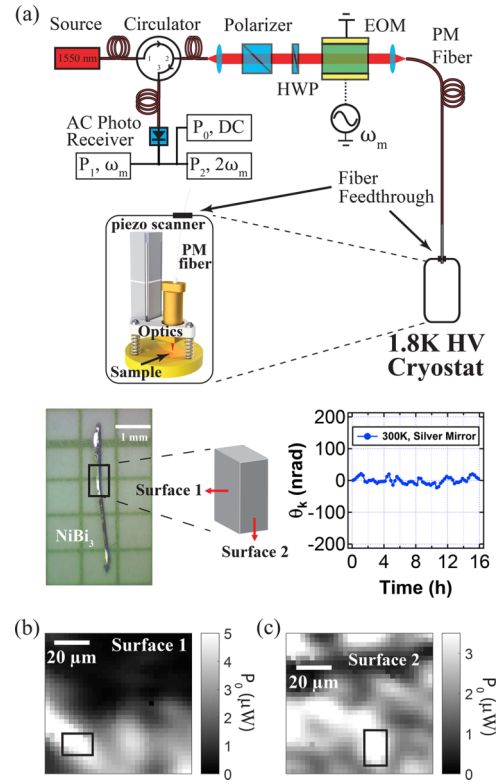

FIG. 1. Sagnac interferometer and $NiBi_3$ crystal. (a) Schematics of a scanning Sagnac microscope at 1550 nm wavelength (top), $NiBi_3$ crystal (left) and 16-h Sagnac drift test on a silver mirror showing 10 nrad Kerr resolution (right). (b) and (c) Reflected optical power (P_0) map at 1.8 K on surfaces 1 and 2, with black boxes marking optically flat regions for measurements.

III. RESULTS AND DISCUSSIONS

Needle-shaped $NiBi_3$ single crystals were grown using the self-flux method with the b axis along the longest dimension [Fig. 1(a)] as determined by x-ray diffractometry [23]. The typical size of such a single crystal is $\sim 3 \times 0.2 \times 0.2$ mm. Figure 2(a) shows the measured resistivity ρ of the $NiBi_3$ sample near the superconducting transition, with the excitation current flowing along the b axis. Here, $T_C = 4.05$ K is determined as the middle point of the resistivity drop and is in good agreement with the result in Ref. [23] on the same batch of crystals. The specific heat (C_p) is shown in Fig. 2(b), with C_p/T vs T^2 plotted near T_C in the inset. A prominent kink at $\sim$4 K indicates a sudden change in the Fermionic contributions to C_p and confirms the superconducting transition. We note that anomalies in $C_p \sim 2.2$ K have been reported [21] in $NiBi_3$ due to amorphous Ni impurities, but we observe no such anomaly in our C_p data, attesting to the high quality of crystals used in this paper.

SMOKE measurements are performed on two lateral surfaces of the crystal, dubbed surfaces 1 and 2, which are perpendicular to the a and c axes, as shown in Fig. 1(a). Due to the softness of the crystal, the surfaces of as-grown

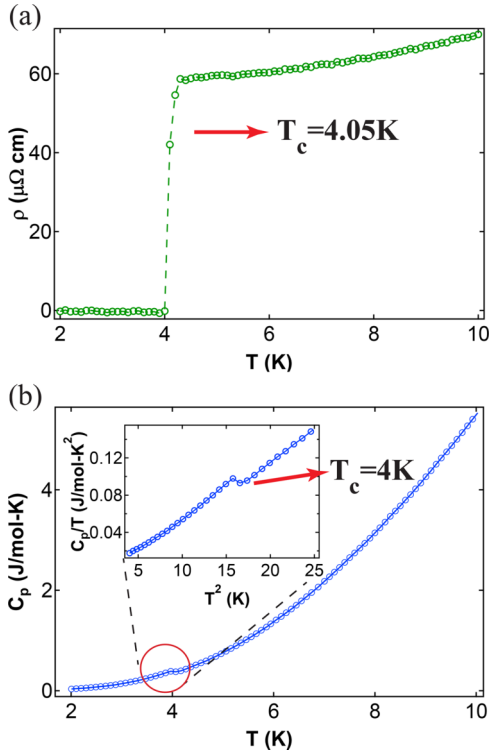

FIG. 2. Resistivity and specific heat. (a) Resistivity (ρ) of $NiBi_3$, where $T_C \sim 4$ K is determined as the middle point of the resistivity drop. (b) Specific heat (C_p) with a kink at T_C. The inset shows C_p/T vs T^2 near T_C.

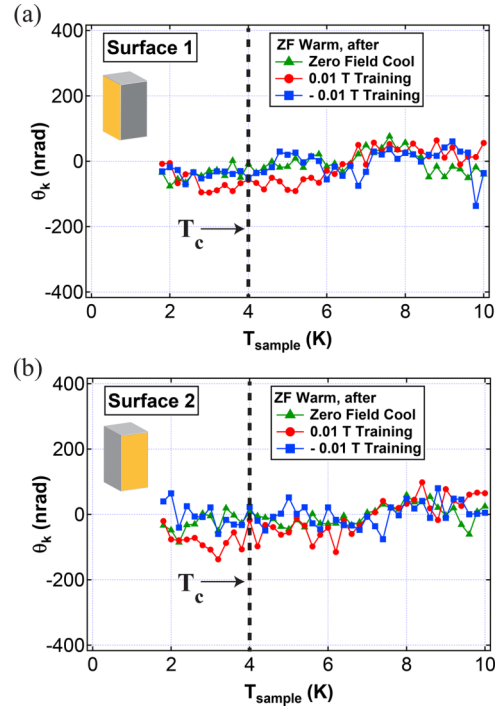

FIG. 3. Absence of time-reversal symmetry breaking (TRSB) in the superconducting state. Kerr signals measured on (a) surface 1 and (b) surface 2 during zero-field (ZF) warmups, after ZF cooldown or after ±0.01 T field trainings, showing no TRSB.

crystals are curved. It is necessary to perform low-temperature scanning imaging to locate optically flat regions for SMOKE measurements. Figures 1(b) and 1(c) are images of reflected light power (P_0) from surfaces 1 and 2, respectively, and optically flat regions marked by black boxes are chosen for SMOKE measurements with $P_0 \sim 5$ μW.

To test possible spontaneous TRSB in the superconducting state, we perform SMOKE measurements at fixed locations on surfaces 1 and 2 during zero-magnetic-field (ZF) warmups. Kerr signals θ_K of such ZF warmups after ZF cooling are presented as green curves in Figs. 3(a) and 3(b), showing no sign of TRSB with an uncertainty of 20 nrad across T_C. As is typical of spontaneous TRSB, the sign and size of θ_K at ZF normally vary as a function of location and temperature. Therefore, a small training field $B_{training}$ is often applied and then removed to align the chiral domains in SMOKE measurements of unconventional superconductors such as in the studies of Sr_2RuO_4 [5], UPt_3 [32], and UTe_2 [33] to name a few. It is noted that, in all these examples, $B_{training}$ is chosen to be smaller than the lower critical field H_{C1} to avoid introducing vortices that can be trapped at pinning sites even after the removal of the training fields. Trainings with $B_{training} > H_{C1}$ could result in nonzero θ_K during ZF warmups due to contributions from trapped vortices, such as those found in $YBa_2Cu_3O_{6+x}$ with a 4 T training field [34]. We pick $B_{training} = \pm 0.01$ T for $NiBi_3$, which is smaller than the measured value [20] of $H_{C1} = 0.015$ T. Kerr signal θ_K during ZF warmups after ±0.01 T trainings are plotted as red and blue curves in Figs. 3(a) and 3(b) for surfaces 1 and 2, respectively: no spontaneous θ_K is observed across T_C with an uncertainty of 20 nrad. In comparison, in epitaxial Bi/Ni bilayers of 20 nm thickness [12], we have detected $\theta_K \sim 120$ nrad onsetting abruptly at $T_C = 4.1$ K [12]. We can therefore conclude that there is no sign of spontaneous TRSB in the superconducting state of single-crystal $NiBi_3$. Furthermore, it was found in sputtered Bi/Ni bilayers that the $NiBi_3$ impurity phase has a preferred orientation of (203) [18]. This translates to a crystalline surface parallel to the b axis, which corresponds to either surface 1 or 2 measured here. Therefore, we could rule out TRSB superconductivity in sputtered and PLD Bi/Ni bilayers where $NiBi_3$ is responsible for superconductivity [17,18].

Now we turn to tests of possible ferromagnetism in $NiBi_3$ that could be induced by either surface effects [22] or extrinsic Ni impurities [21]. As explained earlier, heat capacity C_p [Fig. 2(b)] in our samples indicates a much lower impurity level than those used in Ref. [21], and unlike bulk SQUID magnetometry, Sagnac probes an optical volume of only ~ 0.1 μm^3, making it much less susceptible to Ni impurities.

We first perform magnetic hysteresis measurements with magnetic fields up to ±1 T, which is like the conditions in Ref. [22]. These are shown in Fig. 4(a) for $T = 1.8$ K $< T_C$ (blue) and $T = 10$ K $> T_C$ (yellow). The Kerr signals are extremely linear with the magnetic field B. They are dominated by the background Faraday effect contribution from the low-temperature objective lens, which is proportional to B. The higher noise level $\Delta\theta_K$ comes from the fluctuations in the above lens contribution induced by magnetic field noise. Here, $\Delta\theta_K \sim 5$ μrad at high magnetic fields can be seen

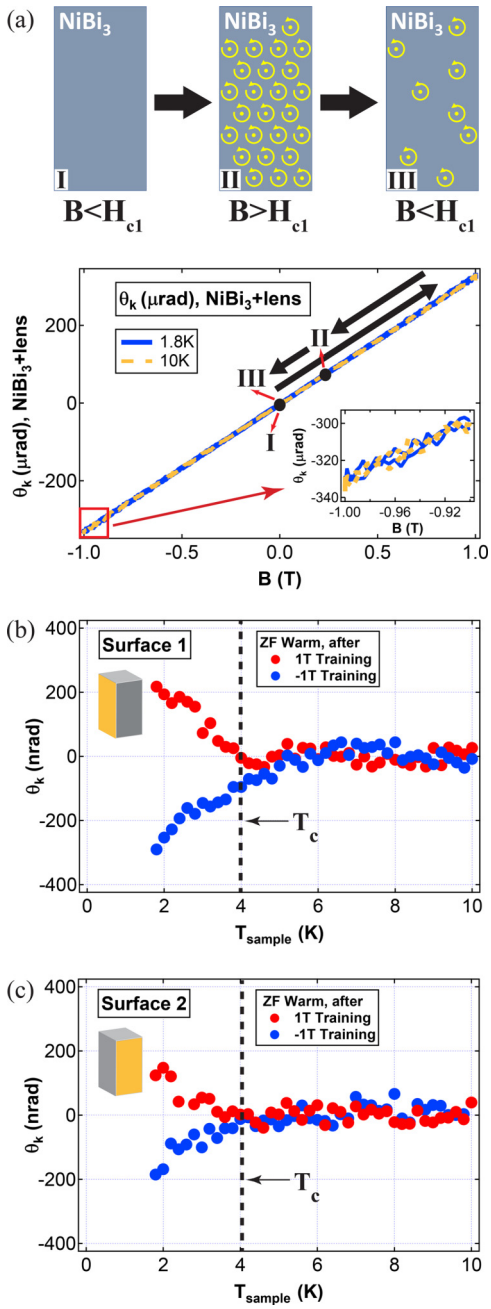

FIG. 4. Trapped vortices and absence of ferromagnetism. (a) Illustration of trapped vortices after removal of a magnetic field $> H_{C1}$ (top); Kerr signals during 1 T magnetic field hysteresis on surface 2 at 1.8 and 10 K (bottom). (b) and (c) Kerr signals measured during zero-field warmups after removing ± 1 T field on surfaces 1 and 2, respectively, showing $\theta_K \sim \pm 200$ nrad onsetting at T_C due to trapped vortices. There is no sign of any ferromagnetism.

in the inset of Fig. 4(a) for θ_K taken between $B = -1$ and -0.9 T. Unlike in Refs. [21,22], we observe no sign of any ferromagnetic hysteresis with 5 μrad uncertainty. It is worth noting that, using the same instrument, we have measured $\theta_K \sim 130$ μrad in 2 nm of Ni [12] and $\theta_K \sim 500$ μrad in 4 nm of $SrRuO_3$ [30]. Therefore, this is already a strong constraint on any ferromagnetism in $NiBi_3$.

For an even more stringent test of ferromagnetism, we measure the remanent Kerr signal by reducing the 1 T magnetic field back to zero at $T = 1.8$ K, as shown in the sequence I-II-III in Fig. 4(a). $NiBi_3$ is a type-II superconductor with a lower critical field $H_{C1} = 0.015$ [20] and an upper critical field $H_{C2} = 0.35$ T [20]. As illustrated in the cartoon in Fig. 4(a), when $H_{C1} < B < H_{C2}$, vortices penetrate the superconducting sample. Their contributions to θ_K are linear with the magnetic field but are overwhelmed in the hysteresis measurements [Fig. 4(a)] by the much larger Faraday effect of the objective lens. After the magnetic field is removed (step III), a small fraction of vortices can be trapped at pinning sites, and they will contribute to θ_K during subsequent ZF warmups. The contribution of the trapped vortices to θ_K would decrease exponentially as the temperature is raised toward T_C. The remanent Kerr signals during ZF warmups after ± 1 T trainings are plotted in Fig. 4(b) for surface 1 and in Fig. 4(c) for surface 2. There are clear remanent Kerr signals of $\theta_K \sim \pm 200$ nrad onsetting sharply at T_C due to trapped vortices. However, we observe no sign of any ferromagnetism with 20 nrad uncertainty, unless its Curie temperature coincides precisely with T_C, which is highly unlikely. We note that the 20 nrad uncertainty is four orders of magnitude smaller than the measured θ_K values in 2 nm of Ni [12] or 4 nm of $SrRuO_3$ [30], strongly indicating that ferromagnetism is absent in $NiBi_3$. Therefore, the reported ferromagnetism in nanostrains [22] of $NiBi_3$ is not due to the surface of $NiBi_3$ but must originate from other sources that are likely irrelevant to Bi/Ni bilayers.

IV. SUMMARY

In summary, we have provided strong error bounds of 20 nrad for any spontaneous Kerr signals in single-crystal $NiBi_3$, strongly indicating the absence of TRSB in $NiBi_3$, whether due to the superconducting state or any coexisting ferromagnetism. We can therefore conclude that the superconducting phases in epitaxial and nonepitaxial Bi/Ni bilayers are distinctively different. In nonepitaxial Bi/Ni, superconductivity originates from the formation of an impurity $NiBi_3$ phase [17,18], which does not host coexisting ferromagnetic order or TRSB superconductivity. In contrast, the epitaxial Bi/Ni samples such as those grown by MBE host a superconducting state that is most likely of chiral p-wave based on existing experimental evidence [12,13]. The latter can be a promising platform for hosting Majorana particles useful for topologically protected quantum computing. It is important to refine the growth process [17] to enable epitaxial growth, especially for non-MBE growth methods, to stabilize and optimize the chiral p-wave state for exploring Majorana physics for robust quantum computing applications.

ACKNOWLEDGMENTS

Experiments at UC Irvine were supported by National Science Foundation Award No. DMR-1807817 and in part by the Gordon and Betty Moore Foundation through Grant No. GBMF10276 to J.X. The work at Hefei was supported by the Youth Innovation Promotion Association

of CAS (Grant No. 2021117). The work at Shanghai was supported by the National Nature Science Foundation of China (NSFC) through Grants No. 11421404 and No. 12004075.

[1] C. Nayak, S. H. Simon, A. Stern, M. Freedman, and S. Das Sarma, Non-Abelian anyons and topological quantum computation, Rev. Mod. Phys. **80**, 1083 (2008).

[2] A. P. Mackenzie and Y. Maeno, The superconductivity of Sr_2RuO_4 and the physics of spin-triplet pairing, Rev. Mod. Phys. **75**, 657 (2003).

[3] A. J. Leggett, A theoretical description of the new phases of liquid He_3, Rev. Mod. Phys. **47**, 331 (1975).

[4] G. M. Luke, Y. Fudamoto, K. M. Kojima, M. I. Larkin, J. Merrin, B. Nachumi, Y. J. Uemura, Y. Maeno, Z. Q. Mao, Y. Mori *et al.*, Time-reversal symmetry-breaking superconductivity in Sr_2RuO_4, Nature (London) **394**, 558 (1998).

[5] J. Xia, Y. Maeno, P. T. Beyersdorf, M. M. Fejer, and A. Kapitulnik, High Resolution Polar Kerr Effect Measurements of Sr_2RuO_4: Evidence for Broken Time-Reversal Symmetry in the Superconducting State, Phys. Rev. Lett. **97**, 167002 (2006).

[6] V. Grinenko, S. Ghosh, R. Sarkar, J.-C. Orain, A. Nikitin, M. Elender, D. Das, Z. Guguchia, F. Brückner, M. E. Barber *et al.*, Split superconducting and time-reversal symmetry-breaking transitions in Sr_2RuO_4 under stress, Nat. Phys. **17**, 748 (2021).

[7] A. Pustogow, Y. Luo, A. Chronister, Y.-S. Su, D. A. Sokolov, F. Jerzembeck, A. P. Mackenzie, C. W. Hicks, N. Kikugawa, S. Raghu *et al.*, Constraints on the superconducting order parameter in Sr_2RuO_4 from oxygen-17 nuclear magnetic resonance, Nature (London) **574**, 72 (2019).

[8] Y.-S. Li, M. Garst, J. Schmalian, S. Ghosh, N. Kikugawa, D. A. Sokolov, C. W. Hicks, F. Jerzembeck, M. S. Ikeda, Z. Hu *et al.*, Elastocaloric determination of the phase diagram of Sr_2RuO_4, Nature (London) **607**, 276 (2022).

[9] J. S. Moodera and R. Meservey, Superconducting phases of Bi and Ga induced by deposition on a Ni sublayer, Phys. Rev. B **42**, 179 (1990).

[10] P. LeClair, J. S. Moodera, J. Philip, and D. Heiman, Coexistence of Ferromagnetism and Superconductivity in Ni/Bi Bilayers, Phys. Rev. Lett. **94**, 037006 (2005).

[11] J. Wang, X. Gong, G. Yang, Z. Lyu, Y. Pang, G. Liu, Z. Ji, J. Fan, X. Jing, C. Yang *et al.*, Anomalous magnetic moments as evidence of chiral superconductivity in a Bi/Ni bilayer, Phys. Rev. B **96**, 054519 (2017).

[12] X. Gong, M. Kargarian, A. Stern, D. Yue, H. Zhou, X. Jin, V. M. Galitski, V. M. Yakovenko, and J. Xia, Time-reversal symmetry-breaking superconductivity in epitaxial bismuth/nickel bilayers, Sci. Adv. **3**, e1602579 (2017).

[13] P. Chauhan, F. Mahmood, D. Yue, P.-C. Xu, X. Jin, and N. P. Armitage, Nodeless Bulk Superconductivity in the Time-Reversal Symmetry Breaking Bi/Ni Bilayer System, Phys. Rev. Lett. **122**, 017002 (2019).

[14] F. S. Bergeret, A. F. Volkov, and K. B. Efetov, Odd triplet superconductivity and related phenomena in superconductor-ferromagnet structures, Rev. Mod. Phys. **77**, 1321 (2005).

[15] S.-P. Chao, Superconductivity in a Bi/Ni Bilayer, Phys. Rev. B **99**, 064504 (2019).

[16] V. Siva, K. Senapati, B. Satpati, S. Prusty, D. K. Avasthi, D. Kanjilal, and P. K. Sahoo, Spontaneous formation of superconducting $NiBi_3$ phase in Ni-Bi bilayer films, J. Appl. Phys. **117**, 083902 (2015).

[17] L. Y. Liu, Y. T. Xing, I. L. C. Merino, H. Micklitz, D. F. Franceschini, E. Baggio-Saitovitch, D. C. Bell, and I. G. Solórzano, Superconductivity in Bi/Ni bilayer system: Clear role of superconducting phases found at Bi/Ni interface, Phys. Rev. Mater. **2**, 014601 (2018).

[18] M. Vaughan, N. Satchell, M. Ali, C. J. Kinane, G. B. G. Stenning, S. Langridge, and G. Burnell, Origin of superconductivity at Nickel-Bismuth interfaces, Phys. Rev. Res. **2**, 013270 (2020).

[19] G. J. Zhao, X. X. Gong, P. C. Xu, B. C. Li, Z. Y. Huang, X. F. Jin, X. D. Zhu, and T. Y. Chen, Singlet superconductivity in a single-crystal $NiBi_3$ superconductor, Supercond. Sci. Tech. **31**, 125005 (2018).

[20] J. Kumar, A. Kumar, A. Vajpayee, B. Gahtori, D. Sharma, P. K. Ahluwalia, S. Auluck, and V. P. S. Awana, Physical property and electronic structure characterization of bulk superconducting Bi_3Ni, Supercond. Sci. Tech. **24**, 085002 (2011).

[21] B. Silva, R. F. Luccas, N. M. Nemes, J. Hanko, M. R. Osorio, P. Kulkarni, F. Mompean, M. García-Hernández, M. A. Ramos, S. Vieira *et al.*, Superconductivity and magnetism on flux-grown single crystals of $NiBi_3$, Phys. Rev. B **88**, 184508 (2013).

[22] T. Herrmannsdörfer, R. Skrotzki, J. Wosnitza, D. Köhler, R. Boldt, and M. Ruck, Structure-induced coexistence of ferromagnetic and superconducting states of single-phase Bi_3Ni seen via magnetization and resistance measurements, Phys. Rev. B **83**, 140501(R) (2011).

[23] X. Zhu, H. Lei, C. Petrovic, and Y. Zhang, Surface-induced magnetic fluctuations in a single-crystal $NiBi_3$ superconductor, Phys. Rev. B **86**, 024527 (2012).

[24] Z. Qiu, Surface magneto-optic Kerr effect (SMOKE), J. Magn. Magn. Mater. **200**, 664 (1999).

[25] S. D. Bader, SMOKE, J. Magn. Magn. Mater. **100**, 440 (1991).

[26] J. Xia, P. T. Beyersdorf, M. M. Fejer, and A. Kapitulnik, Modified Sagnac interferometer for high-sensitivity magneto-optic measurements at cryogenic temperatures, Appl. Phys. Lett. **89**, 062508 (2006).

[27] G. Sagnac, On the proof of the reality of the luminiferous aether by the experiment with a rotating interferometer, Comptes Rendus **157**, 1410 (1913).

[28] A. Kapitulnik, J. Xia, E. Schemm, and A. Palevski, Polar Kerr effect as probe for time-reversal symmetry breaking in unconventional superconductors, New J. Phys. **11**, 055060 (2009).

[29] C. Gong, L. Li, Z. Li, H. Ji, A. Stern, Y. Xia, T. Cao, W. Bao, C. Wang, Y. Wang *et al.*, Discovery of intrinsic ferromagnetism in two-dimensional van der Waals crystals, Nature (London) **546**, 265 (2017).

[30] S. Thomas, B. Kuiper, J. Hu, J. Smit, Z. Liao, Z. Zhong, G. Rijnders, A. Vailionis, R. Wu, G. Koster *et al.*, Localized Control of Curie Temperature in Perovskite Oxide Film by Capping-Layer-Induced Octahedral Distortion, Phys. Rev. Lett. **119**, 177203 (2017).

[31] J. Siegel, J. Witt, N. Venturi, and S. Field, Compact large-range cryogenic scanner, Rev. Sci. Instrum. **66**, 2520 (1995).

[32] E. R. Schemm, W. J. Gannon, C. M. Wishne, W. P. Halperin, and A. Kapitulnik, Observation of broken time-reversal symmetry in the heavy-fermion superconductor UPt_3, Science **345**, 190 (2014).

[33] I. M. Hayes, D. S. Wei, T. Metz, J. Zhang, Y. S. Eo, S. Ran, S. R. Saha, J. Collini, N. P. Butch, D. F. Agterberg *et al.*, Multicomponent superconducting order parameter in UTe_2, Science **373**, 797 (2021).

[34] J. Xia, E. Schemm, G. Deutscher, S. A. Kivelson, D. A. Bonn, W. N. Hardy, R. Liang, W. Siemons, G. Koster, M. M. Fejer *et al.*, Polar Kerr-Effect Measurements of the High-Temperature $YBa_2Cu_3O_{6+x}$ Superconductor: Evidence for Broken Symmetry near the Pseudogap Temperature, Phys. Rev. Lett. **100**, 127002 (2008).